

Angle of Arrival and Centimeter Distance Estimation on a Smart UWB Sensor Node

Tobias Margiani, Silvano Cortesi, *Student Member*, Milena Keller, Christian Vogt, *Member*, IEEE, Tommaso Polonelli, *Member*, IEEE, Michele Magno, *Senior Member*, IEEE

Abstract—Accurate and low-power indoor localization is becoming more and more of a necessity to empower novel consumer and industrial applications. In this field, the most promising technology is based on Ultra-Wideband (UWB) modulation; however, current UWB positioning systems do not reach centimeter accuracy in general deployments due to multi-path and non-isotropic antennas, still necessitating several fixed anchors to estimate an object's position in space. This paper presents an in-depth study and assessment of Angle of Arrival (AoA) UWB measurements using a compact, low-power solution integrating a novel commercial module with Phase Difference of Arrival (PDoA) estimation as integrated feature. Results demonstrate the possibility of reaching centimeter distance precision and 2.4° average angular accuracy in many operative conditions, e.g., in a 90° range around the center. Moreover, integrating the channel impulse response, the phase differential of arrival, and the point-to-point distance, an error correction model is discussed to compensate for reflections, multi-paths, and front-back ambiguity.

Index Terms—UWB, Localization, IoT, AoA, PDoA, Machine Learning, Neural Network

I. INTRODUCTION

Today, precise and low-power indoor localization of mobile devices is still an open problem for both consumer and Machine-to-Machine (M2M) applications [1]. Context and environmental awareness have been recognized as fundamental properties [2] in the Internet of Things (IoT) ecosystem, not only by sensing the surroundings but also by estimating the spatial position regarding reference points and other IoT agents [3]. In many application scenarios, relative and absolute location information are essential features, such as robotics, smart cities and smart manufacturing [2], [4].

Currently, one of the challenges for indoor positioning is to find a sufficiently accurate indoor location method and, thus, a fitting technology [5] valid for extended areas, robust to changes to environmental conditions, scalable to support thousands of devices [6], and, at the same time, capable of working on battery supplied devices [7]. The usage of radio waves for indoor localization has proven to be one of the most solid methodologies, especially in the IoT ecosystem, where the same interface enables data transfer and localization [7]. In this context, Ultra-Wideband (UWB) is one of the most used pivotal technologies to overcome challenges related to the Real-Time Localization (RTL) of

objects in Global Positioning System (GPS)-denied areas. UWB promises localization with centimeter, or even sub-centimeter [8] accuracy, while consuming milliwatts of power and being computationally lightweight [7] - two prerequisites for IoT devices. So far, UWB could only provide a scalar distance l between two ranging agents, ignoring the direction of the incoming signals. However, recent advances [9], [10] demonstrate the possibility of extracting vectorial information \vec{l} , thus providing two characteristics, distance l and direction ψ , to the agent used as a reference point for estimating the spatial position. A vectorial point-to-point distance \vec{l} leads to an improved localization accuracy or/and allows for a decreased number of reference points to localize an object in three-dimensional (3D) space [9], [11]. In this direction, multiple approaches based on UWB technology have been explored. Namely, Angle of Arrival (AoA), Phase Difference of Arrival (PDoA), Time of Flight (ToF), Time Difference of Arrival (TDoA), and Return Time of Flight (RToF) are techniques that show improved localization performance [12]. However, they often require an array of antennas, limiting the compactness of the designed solution [13]. Many different approaches have been proposed to define a global standard similar to common outdoor technologies, such as GPS and Global Navigation Satellite System (GNSS) [3], exploiting other technologies such as WiFi, Bluetooth Low Energy (BLE), UWB, inertial sensors and others [1], [14], [15]. However, today there are no ready-to-use solutions for indoor localization that have been proven to be low-power, scalable, miniaturized, cheap, and accurate (centimeter precision), leaving this challenging research topic unsolved [1].

Among different Integrated Circuit (IC) manufacturers, such as NXP¹, SPARK Microsystem², Microchip³, and Qorvo⁴, products of the last are some of the most widely used UWB modules, namely Decawave's DWM1000 family [7], [8], [16]. It is a commercial UWB IC that supports ToF measurements to estimate the distance among generic devices. Moreover, by estimating the distances between one node and at least four anchors, a trilateration algorithm can be applied to estimate its location in two-dimensional (2D) and 3D space. However, recent studies [7], [11], [16] have shown that the ranging accuracy is still not reliable in several conditions (i.e., Non-

¹ www.nxp.com/applications/enabling-technologies/connectivity/ultra-wideband-uwv

² www.sparkmicro.com

³ www.microchip.com/en-us/products/wireless-connectivity/ultra-wideband-solutions

⁴ www.qorvo.com

Tobias Margiani, Silvano Cortesi, Milena Keller, Christian Vogt, Tommaso Polonelli and Michele Magno are with the D-ITET Department, ETH Zürich, Zürich, Switzerland (e-mail: {tobiasm, cortesi, milkelle, vogtch, toponelli, magnom}@ethz.ch).

Line-of-Sight (NLOS) or presence of external electromagnetic noise). The recently released DW3xxx family from Qorvo showed an increased accuracy paired with a two-times reduction in power consumption [11]. In detail, the DW3120 and DW3220 UWB transceivers support two-way ranging, TDoA and PDoA implementations, enabling not only the estimation of a scalar distance but the possibility to measure at the same time the received signal's AoA and ToF. Thus, providing a 2D position estimation (\vec{l}) relying on one anchor only. The only alternative UWB module that offers similar AoA capabilities within a single IC is the NXP SR150. In contrast to the Qorvo DW3x20's claimed accuracy of $\pm 5^\circ$ at $\pm 45^\circ$ [17], the NXP SR150 has a maximum error of more than 16° at -45° [18]. Other options for achieving similar accuracies as the DW3x20 are using multiple UWB modules (e.g. two DW1000) and therefore doubling the power consumption.

Optimized for low-power battery-supplied operation, the DW3xxx family is designed to be used in mobile, consumer, and industrial applications [11], [19]. However, at the moment of this paper's writing, no existing investigations or extensive studies demonstrate its effective performance in the field.

Extending on the previous study on UWB localization [11], this work presents a sensor node designed to enable vectorial distance estimation (in 2D) on a compact, low-power, and plug-and-play solution for many different applications, such as indoor localization for robotics, wearable, and IoT. Results show that the AoA accuracy reaches an average of 0.59° in the $\pm 45^\circ$ around the center with a compact $3\text{ cm} \times 3.5\text{ cm}$ Printed Circuit Board (PCB) and an average power consumption of 55 mW while in ranging mode. The sensor node is characterized and assessed through a set of data collected in real operational environments, discussing its strengths and weakness, such as front-back ambiguity around 180° AoA. Different error compensation methodologies are proposed, demonstrating the possibility of correcting the measurement uncertainty with a non-linear regression model (up to $35\times$ improvement in accuracy) or classifying reliable operative zones to invalidate values collected outside the confidence interval ($>90\%$ classification accuracy). In detail, the scientific content of this paper includes: (i) Theoretical and background study to enable the AoA estimation over the standard UWB Two-Way Ranging (TWR) protocol; (ii) Design and implementation of a compact sensor node for vectorial distance measurements \vec{l} exploiting the Qorvo DW3220 in a dual antenna setup; (iii) A dataset including several thousand points collected in real operative conditions, acquired at 1° incremental AoA steps for 11 distances in a point-to-point TWR configuration; (iv) A system-level characterization reporting the measurement accuracy in each studied operational condition, including observed boundaries, measurement stability, and repeatability; (v) Based on the physical characterization, error correction methodologies are discussed, demonstrating the possibility of compensating for non-linear system behavior through regression and classification models.

This work can drive future researchers and engineers to enhance indoor localization systems exploiting 2D vectorial distance measurements \vec{l} in miniaturized and low-power devices, providing a system description and also discussing challenges

and limitations to enable accurate UWB-AoA measurements in the field. Lastly, the PCB design and the dataset are released on GitHub as open-source files⁵.

II. RELATED WORKS

The physical principles of AoA estimation based on radio waves have been known for over 80 years [20]. So far, indoor localization techniques using a single receiver were often based on Software-Defined Radio (SDR) and for the use-case optimally tuned carrier frequencies and bandwidths [21], [22]. In recent years, the availability of low-cost hardware and the need for a reliable and cheap indoor localization system pushed the development of novel technologies [12]. In 2015, Dotlic *et al.* [10] described AoA estimation using UWB with a dual-transceiver board, achieving an estimation error of $<10^\circ$ for angles in $\pm 80^\circ$. Starting with the introduction of BLE Direction Finding in 2019, the market started to push towards a low-cost and widely available technology for AoA estimation using a single transceiver. In the work of Botler *et al.* [23], AoA estimation using UWB is compared against BLE. Although the physical principle for determining the Angle of Arrival is the same for both UWB and BLE, UWB-AoA suffers less from an obstructed Line-of-Sight (LOS) and Rayleigh fading due to the higher bandwidth [10], [24]. Measurements performed by Botler *et al.* from $\pm 90^\circ$ at a 3 m distance between anchor and tag showed that UWB generally achieved an accuracy of up to 5° , despite obstructed LOS and multi-path propagation. In comparison, BLE achieved an average error of almost 25° in an outdoor scenario without obstacles. This shows that for an accurate estimation of the AoA, UWB is the most promising technology to use. In order to minimize the influence of multi-path propagation, we therefore decided to focus on a UWB only AoA estimation.

To further decrease the error from the UWB dual-transceiver approach, originating in scheduling uncertainties of the DW1000, [25] introduced a way to synchronize the two transceivers by reducing the timing jitter. Using an additional timestamp correction, the localization accuracy increased by up to 44.33%. The proposed technique has been tested against five responders concurrently. The achieved AoA error is below 10° in 90% of the measurements. The DW3220 used in our paper adds support for a second antenna and on-chip TDoA and PDoA estimations, thus reducing the timing jitter introduced by the scheduling on two separate transceivers.

In addition to the timing jitter, the indoor environments introduced a significant source of estimation errors (both for distance and angle estimation). Objects within the environment influence wave propagation and cause absorption, diffraction, and multi-path scattering [26]. In [27], authors applied different Machine-Learning (ML) techniques (Convolutional Neural Networks (CNNs) and Support Vector Machines (SVMs)) to detect NLOS conditions directly from Channel Impulse Response (CIR) measurements and compensate for it in ranging applications. Using six receivers, their evaluation took place as the first step in a known environment (corridor). The different deep neural networks achieved a detection accuracy of over

⁵github.com/ETH-PBL/UWB_DualAntenna_AoA

94%, leaving the SVM approaches behind by over 10%. Second, they tried it within a generalized, unknown environment. Also there, the CNN outperformed the SVM by 10%, reaching an accuracy of >90%. In a last industrial setting, they tried to augment the localization accuracy and enhanced the Mean Absolute Error (MAE) of ranging from 17 cm to 12 cm. In [9], the AoA is estimated using a single DW1000. Due to the non-idealities of the antenna, the CIR varies between different AoAs. By performing multiple measurements at the same location but with different antenna orientations, Ledergerber *et al.* could map the CIR to the AoA. The CIR is measured at different angles in $\pm 180^\circ$ and then classified into a maximum of 256 bins using a Neural Network (NN) representing the different angles (resolution of 1.41°). With ten consecutive measurements ($N_{\text{CIR}} = 10$), 90% of the predictions had an absolute error of less than 25° . The predictor is then applied to localize a mobile robot, using multiple transmitters and a particle filter to track the robot's position estimation. The overall achieved position estimate had a Root-Mean-Squared (RMS) error of 0.37 m and 3.6° . Instead of classifying the CIR into different bins, [28] applied a deep CNN to perform a regression-based AoA estimation using an N_{CIR} of 5. The ML-based solution outperforms the classical PDoA approach in the range of $\pm 90^\circ$, mainly due to the non-linearity PDoA suffers from around extreme angles. In an experimental setup, including a noisy and multi-path environment, the proposed solution has a 99th percentile error of 2.8° , compared to the 84.5° of PDoA. In this paper, we combine these two ML approaches to compensate for non-idealities, by first splitting the angles into bins/zones and then applying error corrections optimized for each specific zone.

III. AOA ESTIMATION

The distance between two UWB transceivers is estimated based on the ToF of the wireless signal.

In addition to the distance measurement, the DW3220 IC can measure TDoA and PDoA. The TDoA indicates the timestamp difference of the same signal arriving at the two antennas. Since the typical antenna spacing (d in Fig. 1) is half a wavelength or closer, a typical TDoA value is below 1 ns. On the other side, the PDoA measures the difference in signal phase (due to additional travel distance p in Fig. 1) between the first antenna and the same signal arriving at the second antenna. With appropriate antenna placement, the AoA (ψ) is strictly correlated with the PDoA. Thus, the planar (2D) AoA can be calculated from the PDoA α , using a geometrical approach shown in Fig. 1 and expressed in Eq. 1, with the carrier wavelength defined as λ .

$$\psi = \arcsin \frac{\alpha \lambda}{2\pi d} \quad (1)$$

There are two points to note when using a dual antenna system to estimate the AoA. First, by using only the PDoA measurement, it is impossible to differentiate between signals arriving from the "front" of the module and those arriving from the "back". This effect is called front-back ambiguity [25], and limits the absolute angle measurement to 2D and $\pm 90^\circ$.

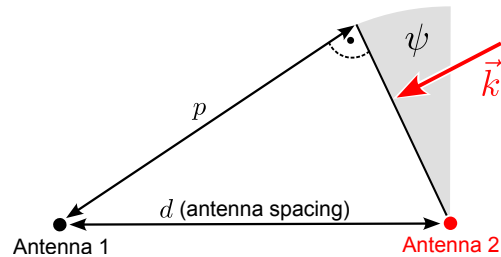


Fig. 1: Dual antenna setup with distance between the antennas d , actual angle of arrival ψ , incident plane wave (vector \vec{k}) and resulting antenna signal phase difference caused by additional travel distance p .

Second, for accurate localization, the distance and AoA measurements must result from signals traveling on a LOS path. Otherwise, the incoming signal can result from a multi-path, thus arriving from a completely different direction. Hence, it becomes clear that a compensation algorithm, or a system with > 2 antennas, can be beneficial to correct the aforementioned source of inaccuracies, also enlarging system boundaries to cover the entire 360° range.

IV. HARDWARE DESCRIPTION

The hardware used in the proposed system is split into three main components. First, an STM32-based Microcontroller Unit (MCU) board from STMicroelectronics (later referred to as host MCU) interfacing with the UWB transceiver and a computer for data collection. Second, a custom PCB containing a Qorvo DW3220 UWB transceiver connected to two antennas (later referred to as double antenna module). Lastly, a Qorvo DWM3000EVB board with a Qorvo DW3110 transceiver and a single antenna as a communication counterpart to the custom dual antenna module (later referred to as single antenna module) was used alternatively as an anchor or tag depending on the specific test setup. The choice of an STM32 MCU allows for rapid development using the Qorvo UWB IC and easy integration into future low-power localization applications.

A. DW3220 UWB Module

The Decawave/Qorvo DW3220⁶ IC is a low-power IEEE 802.15.4-2015 compatible UWB transceiver released in 2020. It is the successor of the widely used Decawave DW1000 IC [29], adding support for a second antenna and on-chip TDoA and PDoA estimations. The claimed typical accuracy is ± 6 cm for ranging and $\pm 10^\circ$ for PDoA⁶ estimation in LOS conditions. While there has been a range of research on using multiple antennas to improve localization [28], the DW3220 IC is, to the best of our knowledge, the first supporting two antennas and PDoA estimation in a single compact package and optimized power consumption. The DW3000 series of ICs supports UWB channels 5 and 9, data rates of 850 kbps and 6.8 Mbps, Scrambled Timestamp Sequences (STS) for secure ranging, and multiple low-power states. The DW3220 has

⁶www.qorvo.com/products/p/DW3220

two antenna ports internally connected to a Radio Frequency (RF) switch and a single radio front end. The switch is automatically controlled in hardware to sample the CIR data from both antennas and measure TDoA and PDoA. This automatic switch control is only possible if the incoming data packet contains an STS frame, a feature added with IEEE 802.15.4z, which therefore is not compatible with the older DW1000 IC. A single IC with two antenna ports eliminates the need for pico-second time synchronization between multiple receivers, which would otherwise be required for TDoA and PDoA estimation. Additionally, it reduces the Bill of Material (BOM), simplifies dual antenna designs, optimizes power consumption (e.g., $4\times$ reduction compared to [28]), and results in a potentially higher accuracy by eliminating timing error sources.

B. Sensor Node

At the moment of this paper's writing, no evaluation boards, commercial products or hardware design documentation is publicly released. Thus, to use the DW3220 IC, a sensor node was designed to support the double antenna configuration and satisfy RF minimal requirements. It is optimized for low power usage and RF quality when UWB channel 5 (6.5 GHz) is used. Two chip antennas are spaced at $1/2$ wavelength to allow accurate PDoA estimation - a design specification from a previous study [10].

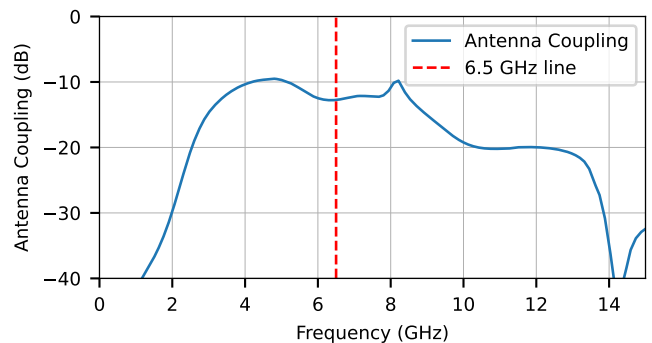
The power supply is divided into two voltage regulators with a dedicated direct current (DC)/DC converter each. The external power supply is connected to the module through a castellated connector. It is linked to the first buck converter, TPS62233DRYR, which generates an output voltage of 3V. This feeds the DW3220 VDD1 main power supply, which supplies the device inputs/outputs (I/Os) and the always-on domain. The 3V line powers the second buck converter TPS62743YFPR with a fixed DC output voltage of 1.8V, connected to the VDD3 pin. The TPS62743YFPR is controlled by the DW3220, which can enable or disable the RF power supply in real time - depending on the operational mode. Using this scheme, the most efficient power consumption setting is achieved.

As explained in Section III, the antennas must be separated by $\lambda/2$ to reach the best accuracy. We use channel 5 with a nominal frequency of $f = 6.4896$ GHz and therefore an antenna spacing of $d = c/(2 * f) = 0.023114 \approx 2.31$ cm. The desired 50Ω impedance target, the microstrip to coplanar waveguide coupling, and the choice of the dielectric material are investigated and simulated to match the DW3220 specs. An S11 of -22 dB was reached with a *ThunderClad 2* substrate material around 6.5 GHz and a bandwidth of 4 GHz @ <-10 dB. The finally selected substrate was *ThunderClad 2* with 0.1068 mm thickness and a trace width of 0.145 mm.

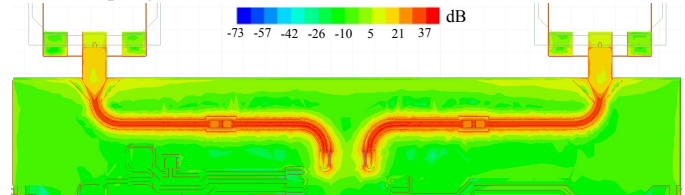
To correctly estimate the antenna's electrical delay and the cross-coupling between the two, together with the radiation pattern, a precise antenna 3D Finite Element Method (FEM) model is required. We selected the commercial integrated Surface Mount Technology (SMD) antenna AH086M555003 manufactured by Taiyo Yuden for our design. The 3D FEM



Fig. 2: Sensor node. Antenna intra-spacing and digital connections are outlined.



(a) Coupling factor between the two AH086M555003 antennas.



(b) Current density distribution over the RF traces, matched at 50Ω and symmetrically placed.

Fig. 3: FEM simulation and modeling of the designed dual antenna PCB. The PCB substrate is *ThunderClad 2* with 0.1068 mm thickness between the RF line and the ground plane. The two antennas are at 2.31 cm distance.

tools ANSYS HFSS⁷ and ANSYS SIwave⁸ were used to additionally simulate the behavior of the RF traces to ensure proper matching between the chip-antennas and the controlled impedance RF traces on the sensor node as well as with the addition of the real antenna model.

Fig. 3a shows the graph of the antenna coupling parameter expressed in decibels. At a frequency of 6.5 GHz, the coupling amounts to -12.55 dB. This parameter is not optimal but

⁷<https://www.ansys.com/products/electronics/ansys-hfss>

⁸<https://www.ansys.com/products/electronics/ansys-siwave>

acceptable for the scope of this work. For future design and developments, a dedicated custom dual-antenna should be considered to decrease, or compensate, for this parasitic effect. Fig. 3b shows the simulated current density distribution in the region of the RF traces. As expected, the traces are conducting most of the energy, expressed by the red color scale corresponding to a high current density. The coupling of the two antennas is visible, as exactly in the middle between the two lines, the current density on the ground plane is not equal to zero and, therefore indicating a non-perfect decoupling.

V. EMPIRICAL CHARACTERIZATION

To demonstrate the possibility of gathering AoA and distance information using a compact integrated sensor, a range of tests were conducted to quantify the performance of the DW3220 IC empirically and, at the same time, collecting a comprehensive dataset to model and compensate for errors and measurement inaccuracies. For all the presented measurements, one single antenna module and one double antenna module were placed in an $8.6\text{ m} \times 7.7\text{ m}$ room containing tables and office equipment placed along the walls and a $6.5\text{ m} \times 5.5\text{ m}$ empty space where the measurements were performed. The single antenna module was fixed on a tripod at a height of 1.1 m. In contrast, the double antenna module was mounted on a rotatable motorized platform, providing a ground truth AoA with a precision of 1° . The modules were configured to perform two-way ranging [11] at a frequency of 4.6 Hz. All measurements were done with LOS visibility between the two UWB modules, and no objects were placed within 1 m of the devices or the LOS signal path.

The two UWB modules continuously exchange TWR frames while a local computer logs each frame received by the double antenna module. The collected data includes the CIR from both antennas, TDoA, PDoA, transmission quality and signal strength indicators, as well as round-trip and reply times from TWR, and the computed distance estimation. All data, except for the TWR information, is directly computed on hardware, therefore, requires no processing on the local MCU.

The dataset used for the system characterization and later error compensation (section VI) contains measurements collected from a total of 19880 exchanges. For data collection, the UWB modules were placed at 11 fixed distances ranging from 50 cm to 5.5 m in 50 cm steps. At each distance, the double antenna module was rotated in 1° steps, and for each of those, at least five TWR measurements were performed.

A. PDoA and AoA

From each collected measurement, an AoA estimation was computed using Eq. 1 and coupled with its ground truth angle. An example of the collected data is shown in Fig. 4, where the device-to-device distance is 3 m. Fig. 4 shows that the AoA estimation curve is linear around $\pm 45^\circ$ and strongly correlates ($r = 0.98$) with the ground truth on the horizontal axis. For angles around $\pm 60^\circ$, a non-linear behavior is apparent, introducing an increase of the average error above 5° . Outside this range, the AoA estimation accuracy drops significantly, losing a visible correlation with the actual rotation. Additionally,

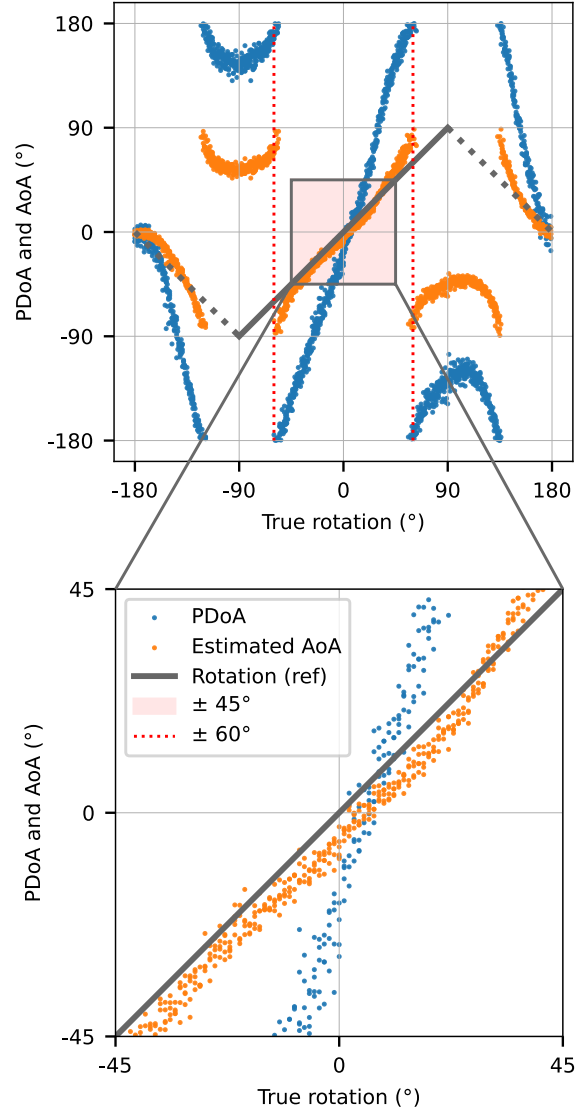


Fig. 4: PDoA measurement and resulting AoA estimation (based on Eq. 1) at a distance of 3 m. Note that the true rotation was a full 360° ; however, due to front-back ambiguity, all estimated AoA values fall between -90° and 90° . Outside of this range, the reference line is dotted, showing the expected AoA estimate instead of continuing straight on the true AoA values.

front-back ambiguity can be observed outside the center $\pm 90^\circ$ range. The PDoA and estimated AoA values turn back towards 0° instead of increasing towards 180° . As this is expected from the physics of the double antenna setup and simulated in Section V-C, the reference line is drawn accordingly (dashed in Fig. 4).

However, despite non-linear behavior and the front-back ambiguity being expected around 90° , results in Fig. 4 show a wide glitch of 63° to 77° starting at $\pm 60^\circ$, equivalent to a variation of the antenna spacing Δd of 7.7 mm. This wrap-around centered at $\pm 90^\circ$ in the PDoA could be caused by several possible factors. Among them, we considered an

incorrect antenna placement (see Fig. 2) during the PCB assembly, which was disproved by observing similar results on two additionally soldered PCBs. A second alternative is the effective antenna center and signal propagation, which was considered an ideal point in the center of the SMD package and, more important, spatially invariant. In reality, the antenna delay and its effective wave incident point can vary depending on the angle of the incoming signal, consequently boosting the front-back ambiguity error on a wider angular range.

Considering only true AoA values from -45° to 45° (as pictured in the zoom of Fig. 4), the AoA estimate reaches a Mean Squared Error (MSE) of only 0.59° and an MAE of 5.21° at a distance of 3 m. For all evaluated distances, the maximum MSE is 2.40° and the maximum MAE 8.46° . Extending the range up to where the wrap-around in PDoA values begins increases the error due to the denoted non-linear behavior. At a 3 m distance and a range of $\pm 60^\circ$, an MSE of 12.00° and MAE of 11.67° is achieved. The precise angle of the wrap-around varies depending on the distance but always lies between 50° and 60° . Another observation based on the collected data is a flattening of the PDoA and AoA curves close to 180° and increased non-linearity towards $\pm 135^\circ$. This can be seen in Fig. 4 by comparing the shape around 0° in the center and 180° on the left and right sides of the plot. The distance from 180° to the wrap-around in PDoA values is only 37° to 47° , whereas the distance from 0° to the wrap-around is 50° to 60° . These considerations demonstrate a decreased accuracy while operating on the back side of the module. In the 90° range from 135° to 225° , an MSE between 13.51° and 23.95° is observed depending on the distance.

An analysis of the raw data originating from the TWR distance measurement will be skipped here, as there are only a few changes compared to the well-studied DW1000 IC, which is already extensively discussed in [11]. The data will, however, be used in section VI to develop a joint error correction model for AoA and TWR distance errors. The collected dataset and the PCB design are released as open source on GitHub for future usage and improvements⁵.

B. Stability

The stability of the AoA estimation provided by the DW3220 is evaluated over different distances and time. As shown by the experimental results in Fig. 5, the PDoA measurements are comparable over all tested distances, between 50 cm and 5.5 m. The MSE and MAE are consistent with the characterization mentioned above at 3 m and within the DW3220 specs. Noticeable differences are the precise point of the wrap-around in PDoA values, which is spread over 25° , and the different inaccuracies around 180° .

To evaluate the stability over time, another set of experiments was performed. The two UWB modules were again placed at a fixed distance, and it was ensured that there was no movement in the room for the duration of each experiment. Over a period of 11 minutes, about 3000 TWR exchanges were performed. This was repeated for AoA of 0° , 90° , 180° and 270° . The resulting PDoA measurements feature no drift over time, with results spread as Gaussian distribution. After

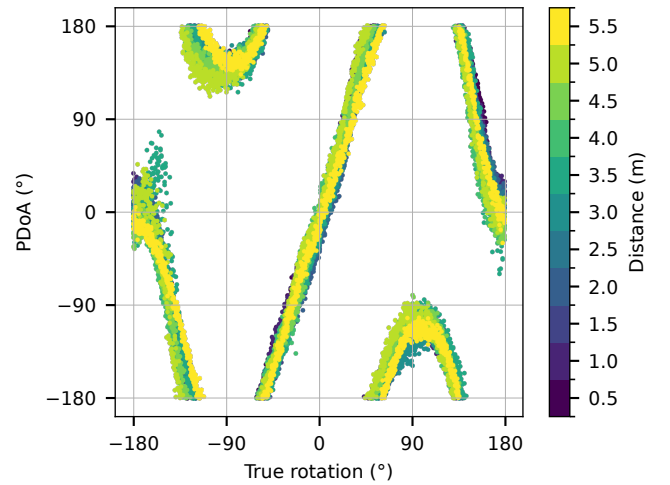


Fig. 5: PDoA measurements for each AoA in 1° steps and each distance between 50 cm and 5.5 m in 50 cm steps.

computing the estimated AoA, a standard deviation of 2.45° is achieved over all tested angles. By averaging 10 AoA estimations, the standard deviation can be reduced to below 1° for all angles, and in the best case ($\psi = 0^\circ$), even below 0.6° . When averaging results, additional considerations are necessary to properly handle values close to the boundaries as, e.g., a true PDoA value close to 180° can also be measured as close to -180° .

C. 3D FEM PCB Simulation

In order to analyze some of the non-idealities encountered during the empirical characterization of the PCB designed in Section IV-B, a 3D FEM simulation was conducted to compare the phase shift between the antennas with known angles of arrival. The PCB design was imported into Ansys HFSS 3D together with a model of the UWB antenna. The environment is a 120 mm-sized vacuum cube with a perfectly matched boundary layer. The simulation is based on a transient composite excitation model with a plane wave source excitation.

The plane wave's phase origin (\vec{O}) is rotated along a circle with a 50 mm radius centered between the two antennas at the PCB simulation origin (see Eq. 2 and the center in Fig. 6). This was chosen as a compromise between the absolute distance of the wave source to the PCB and relative distance difference to the antennas. The incident angle of the wave with respect to the PCB plane normal is defined as ψ .

$$\vec{O} = 50 \text{ mm} \cdot \begin{pmatrix} \sin(\psi) \\ 0 \\ \cos(\psi) \end{pmatrix} \quad (2)$$

The wave propagates along a \vec{k} -vector pointing to this simulation origin (Eq. 3), and the electric field vector points along the y -axis of the simulation.

$$\vec{k} = \begin{pmatrix} -\sin(\psi) \\ 0 \\ -\cos(\psi) \end{pmatrix} \quad (3)$$

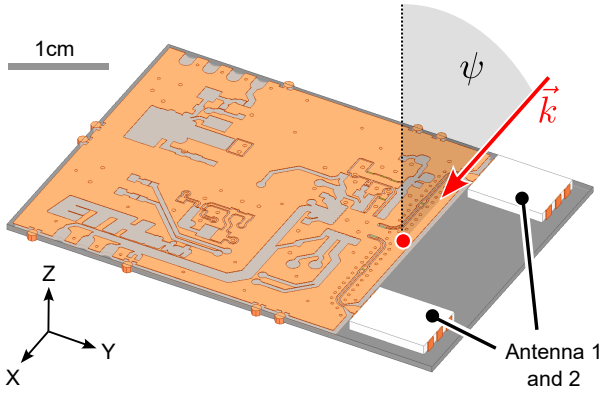


Fig. 6: 3D rendering of the simulated PCB geometry with the origin marked as a red dot between the two antennas and the wave incident angle ψ , as well as an example of the plane wave propagation vector \vec{k} .

The time-dependent electric field magnitude $A(t)$ (Eq. 4) of this plane wave is defined to be a UWB pulse with a bandwidth of ≈ 500 MHz ($\tau = 4$ ns), a center frequency of $f_0 = 6.5$ GHz, and a scale factor G based on [30]. The UWB receiver chip was modeled as lumped element resistors of 50Ω located at the solder pads of the RF input to the chip and referenced to the ground plane next to these pads.

$$A(t) = G \cdot \frac{t}{\tau} \cdot e^{-2\pi(\frac{t}{\tau})^2} \cdot \sin(2\pi f_0 t) \quad (4)$$

During the simulation, ψ varied between 0° and 90° , and the resulting phase shift between the antennas was extracted. The simulation had ≈ 245200 degrees of freedom to solve and a transient time between 0 and 4 ns.

The resulting phase shift with respect to the incident wave is given in Fig. 7. It shows the PDoA phase wrap-around at $\psi \gg 65^\circ$ (Fig. 7a). The insets in Fig. 7b,c present the voltage received at the UWB chip inputs, caused by the incident plane wave. It illustrates the phase-wraparound due to a too-large time (phase) shift between the two antennas. At $\psi = 81.56^\circ$ (Fig. 7c), the time shift between the antennas is 87 ps, corresponding to $\approx 203^\circ$ at $f_c = 6.5$ GHz. Due to the possible solutions of PDoA, this wraps around to $\approx -157^\circ$. Therefore, future PCB designs could be improved by reducing the antenna distance.

VI. POSITION AND ANGLE ERROR COMPENSATION

Despite the promising angle accuracy within $\pm 45^\circ$ around the center, there are apparent deficiencies in directly calculating the AoA from the PDoA. Therefore, this section discusses and evaluates multiple methods to compensate for the observed measurement error. This includes not only the compensation for the non-linearity but also correcting the wrap-around in PDoA measurements and front-back ambiguity.

Initially, a single correction algorithm is considered to generate a compensation curve for the two sources of AoA errors and to calibrate the TWR distance measurement. Different ML approaches are investigated to model the antenna behavior at different wave incident angles and multi-paths in LOS

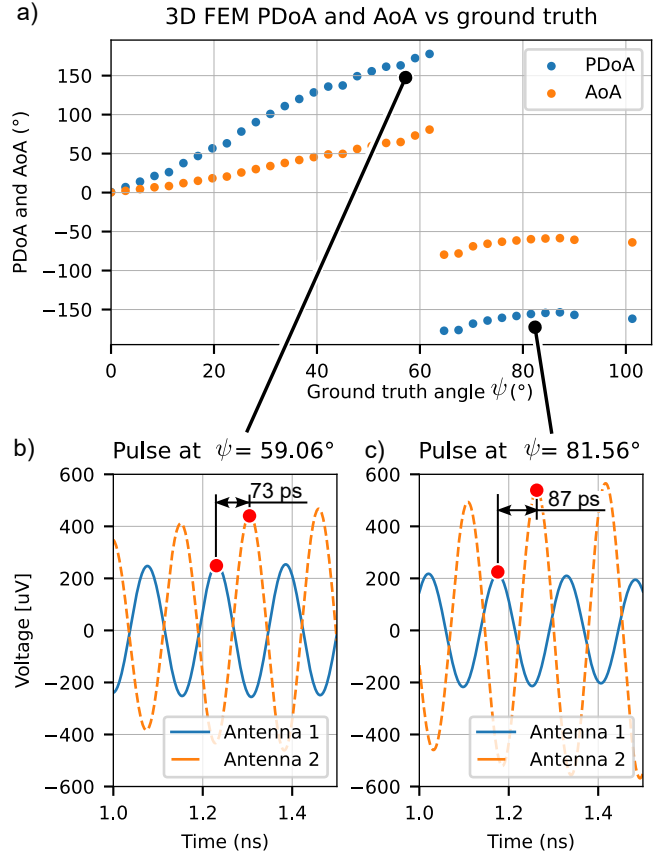


Fig. 7: Resulting phase shift between antennas with respect to known input angle ψ , with an overview of all PDoA and corresponding AoA calculated with Eq. 1 (a), detail TDoA for the wrap-around effect of angles (b,c).

environments. A similar approach has been used in the past for the sole TWR distance estimation setup, for example, to extract the AoA from a single antenna [9] or to detect NLOS conditions [27].

The dataset used for training and assessing different ML models is the same as described in section V. It contains 19880 samples (i.e. TWR exchanges), of which 19508 were used for training and evaluation while the others were excluded for the following reasons: (i) TDoA values above 1 ns; (ii) TWR values below 1000; Both of which indicate measurement errors. The remaining samples were split into 11704 samples for training ("train" dataset) and 7804 samples for model evaluation ("test" dataset). In addition, a secondary dataset ("evaluation" dataset) containing 6651 samples was generated using the same data collection setup but with different environmental conditions, such as different room dimensions, furniture, and exact placement of UWB modules. This evaluation dataset was used to check the models for generalization into different environments.

The error correction algorithms discussed in this work are restricted by computational load and memory size. The evaluated algorithms should finally work in real-time on a host MCU, which typically operates at a frequency of ≈ 100 MHz and provides ≈ 100 kB of memory. Therefore, the proposed

localization system is designed to work independently of the final application and without the support of external computing units, except the host MCU.

A. Models and Data Preprocessing

Two ML methods are investigated, namely gradient boosting (using XGBoost [31]) and Neural Networks ([9], [27], [28]). Many different model architectures are found in the literature, therefore different hyper-parameters were evaluated for each model type, always using the same input features and outputs. Model inputs include PDoA, TDoA and CIR measurements at both antennas, the TWR distance estimate, and the fraction of the total divided by first path power indicators. The TDoA could potentially include information to correct the PDoA wrap-around. In contrast, the CIRs and power indicators potentially include information about the environment, signal quality, and multi-paths, which can support the identification and compensation of antenna non-idealities, including front-back ambiguity. The DW3220 IC provides the CIR as 512 complex samples with 36-bit precision each. A subset of these samples was split into real and imaginary parts to be used as ML input parameters.

The first set of models is trained for regression, outputting predictions of the AoA estimation error and the actual distance between both UWB modules. Hyper-parameters evaluated for XGBoost models include the number of estimators between 25 to 500. For neural networks, the following hyper-parameters are evaluated: (i) the number of layers (1 to 3); (ii) the choice of fully connected layers (32 to 256 nodes); (iii) the usage of a first convolutional layer (using filter sizes from 8 to 128 and kernel sizes from 3 to 11). Additional settings are evaluated during the training, such as average pooling located after the convolutional layer, or dropout layers with varying dropout rates (0.125 to 0.5), and skip connections (ResNet [27]).

The second set of models is trained for classification of wave incident zones. They are defined as 90° wide AoA sections centered around 0° , 90° , 180° , and 270° , hence exactly covering the full circle. The classification is trained and assessed on XGBoost and fully connected neural networks with 1 to 3 layers of 32 to 256 nodes each. Optional dropout layers are re-evaluated as well. Instead of applying for direct compensations, this approach is designed to classify different working zones allowing for subsequent correction of AoA and distance measurements with polynomial fitting curves or completely discarding the acquired sample, e.g., in the case of the 180° zone.

TDoA and PDoA values are scaled to zero mean and unit variance, while the TWR distance estimate was scaled to $[0, 1]$. Of the 512 CIR samples from the DW3220, only those between 5 samples before and 100 samples after the first signal path were used. Initial trials with the full CIR were computed but did not lead to any tangible improvement; therefore the CIR is restricted to decrease the model size and to counteract potential overfitting. The CIR values are scaled to a maximum of 1. As target variables for XGBoost, the AoA estimation error and the true distance were used. In contrast, the results for NN-based models improved by using sine and cosine of the AoA estimation error and the true distance as targets.

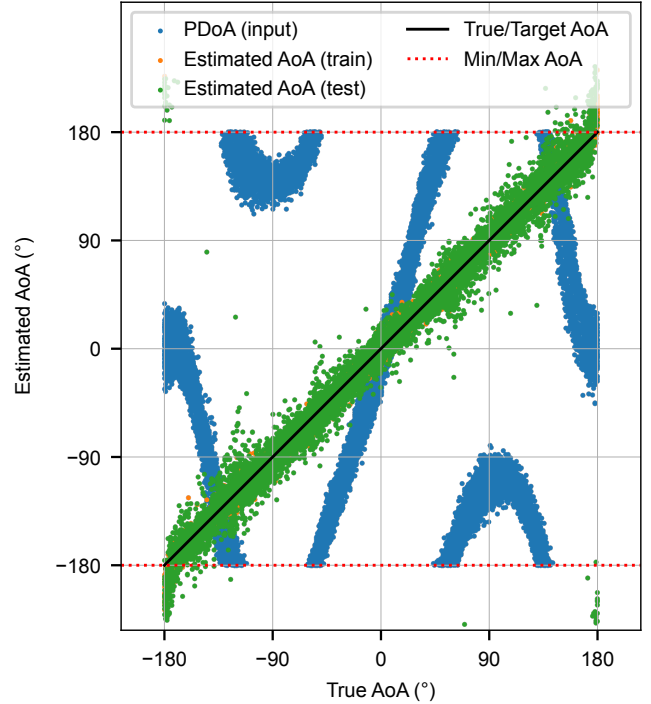


Fig. 8: AoA estimated by a fully connected NN model. The PDoA shows the wrap-around and front-back ambiguity, which is both corrected for by the ML model. Around $\pm 180^\circ$, the variance increases, and some estimates lie outside the possible range of -180° to 180° degrees.

B. Results

Both gradient boosting and NN models were trained with all possible combinations of the above-mentioned hyper-parameters. The two models proposed here were then selected as a trade-off between the simplicity of the model (for computational efficiency on embedded applications), prediction accuracy on train and test sets, and prediction accuracy on the secondary evaluation dataset.

Using gradient boosting, the chosen model contains 100 estimators resulting in a model size of 42 kB. The model predictions achieve an MSE of 3.21° and 43.70° , respectively, on train and test datasets, over the entire 360° range, effectively solving the front-back ambiguity and PDoA wrap-around. The chosen NN model consists of a single-layer fully connected NN with 224 nodes and a size of 373 kB. This results in an MSE of 2.03° and 19.35° on train and test datasets, respectively. As can be seen in Fig. 8, and as expected, the best accuracy is achieved close to 0° , and accuracy is reduced towards 180° , where significant variance can be observed in the results of the test dataset. Additional improvements can be made by discarding results outside the -180° to 180° range, which should never occur. This allows for reaching an MSE of 1.52° and 15.27° on train and test datasets, respectively.

In addition to the AoA, the models corrected the TWR distance estimate. XGBoost reached an MSE of 0.37 cm and 6.25 cm on the train and test datasets, respectively. Using the single-layer neural network, an improved MSE of 0.29 cm on

the train dataset and 2.24 cm on the test dataset has been achieved. To ensure the stability over distance (cf. subsection V-B) the NN model was again trained on each distance separately. Thereby achieving an MSE of between 5.17 and 19.65 for each distance contained in the dataset.

The two models were also assessed on the secondary evaluation dataset to check for possible generalization. This never reached comparable results with the test dataset. Variations in the number of input feature, dropout layers, or skip connections (residual networks) were investigated to reduce overfitting. However, no significant improvement has been noticed. Hence results demonstrate that this methodology is effective for applications where the environment is known *a-priori* or in use cases where a model re-tuning is possible. However, this approach cannot be used for designing plug-and-play and flexible UWB sensor nodes that can operate in several indoor/outdoor environments. Moreover, these findings demonstrate how the models effectively learn to compensate for environmental effects, such as reflections, multi-path, and noise, instead of learning the antenna's physical behavior.

Classification into 90° measurement zones resulted in higher accuracy and better generalization than the regression approach. The XGB classifier achieved perfect precision and recall on the train dataset for all classes. For the center class, precision and recall of 0.98 and 0.98 are achieved on the test dataset and 0.65 and 0.80, respectively, on the evaluation dataset. The fully connected neural network also achieved perfect precision and recall on the train dataset, while on test and evaluation datasets, precision and recall were 0.98, 0.97, and 0.62, 0.87, respectively. This shows the potential of a two-step solution to AoA estimation in changing environments. After estimating the zone, a different method can be used to compute the AoA estimation (e.g. direct estimation with Eq. 1 in the center class).

Finally, regression was performed within the 90° measurement zones. Restricted to one of the three zones not containing 180°, the neural network provided estimations with MSE below 0.8° on train and test datasets and below 8° on the evaluation dataset. On the zone containing 180°, an MSE of 4.86°, 66.62°, and 212.96° was achieved on train, test, and evaluation datasets, respectively. This shows how restricting the operating AoA range can significantly improve the accuracy and generalization of the models. As shown in subsection V-A, direct computation of the AoA using Eq. 1 provides similar results in the center zone. However, the zones at 90° and 270° cannot be computed with the direct approach due to non-linearities and PDoA wrap-around.

VII. CONCLUSION

This paper introduced a novel dual antenna sensor node using the DW3220 IC, thus providing a compact and low-power module for PDoA measurements and AoA-enabled applications. The node was subsequently used to thoroughly evaluate and characterize the UWB IC for AoA estimations under real operating conditions. Finally, error sources in the AoA estimation were identified, and solutions based on different ML models were proposed and evaluated.

Instead of relying on connected and tightly synchronized single antenna modules (i.e. based on the DW1000 IC) for PDoA acquisition, the novel sensor node provides a way to utilize the dual antenna capabilities of the DW3220 IC. This not only simplifies the hardware design and decreases BOM cost but also reduces the number of error sources. As shown, the remaining errors can often be removed using simple and efficient techniques.

The empirical characterization of the DW3220 IC in section V showed high AoA accuracy within the 90° AoA range of -45° to 45°. With an MSE of below 2.41°, the claimed accuracy of the IC of $\pm 5^\circ$ is exceeded. However, the naive approach of computing AoA from PDoA quickly breaks down if the range of tested angles increases. This stems from non-linearities in the measurement, front-back ambiguity, as well as hardware details, as simulated in subsection V-C.

Multiple ML models were evaluated, resulting in the detailed analysis of one based on gradient boosting and one based on neural networks. The models are small in size (21 kB and 373 kB for XGB and NN, respectively) and will enable integration on low-power hardware. They allow accurate estimation of the AoA and distance if trained in the corresponding environment. A physical approach for removing front-back ambiguity is to add a third antenna; however, this might not be necessary as the proposed models could directly correct for that while keeping the MSE well below 20°.

Finally, a two-step solution is proposed if the models cannot be trained in the final environment. First, classification into 90° wide measurement zones and second, AoA estimation within those zones. The second step can, for example, be computed directly from PDoA measurements (Eq. 1) in the zones centered on 0° and 180° AoA, or a specific ML model for each zone can be used. In addition, error-prone measurements in the zone centered on 180° AoA could be discarded.

Possible further research could evaluate the generalizability of ML models using an extended dataset or combine multiple double antenna modules for AoA estimation and localization in a 3D space.

REFERENCES

- [1] G. Cerro, L. Ferrigno, M. Laracca, G. Miele, F. Milano, and V. Pingerna, "Uwb-based indoor localization: How to optimally design the operating setup?" *IEEE Transactions on Instrumentation and Measurement*, vol. 71, pp. 1–12, 2022.
- [2] F. Zafari, A. Gkelias, and K. K. Leung, "A survey of indoor localization systems and technologies," *IEEE Communications Surveys & Tutorials*, vol. 21, no. 3, pp. 2568–2599, 2019.
- [3] K. Zhang, P. Chen, T. Ma, and S. Gao, "On-demand precise tracking for energy-constrained uavs in underground coal mines," *IEEE Transactions on Instrumentation and Measurement*, vol. 71, pp. 1–14, 2022.
- [4] L. Chen, S. Thombre, K. Järvinen, E. S. Lohan, A. Alén-Savikko, H. Leppäkoski *et al.*, "Robustness, security and privacy in location-based services for future iot: A survey," *IEEE Access*, vol. 5, pp. 8956–8977, 2017.
- [5] W. Gifford, D. Dardari, and M. Win, "The impact of multipath information on time-of-arrival estimation," *IEEE Transactions on Signal Processing*, 2020.
- [6] M. Zhao, T. Chang, A. Arun, R. Ayyalasomayajula, C. Zhang, and D. Bharadia, "Uloc: Low-power, scalable and cm-accurate uwb-tag localization and tracking for indoor applications," *Proceedings of the ACM on Interactive, Mobile, Wearable and Ubiquitous Technologies*, vol. 5, no. 3, pp. 1–31, 2021.

- [7] T. Polonelli, Y. Qin, E. M. Yeatman, L. Benini, and D. Boyle, "A flexible, low-power platform for uav-based data collection from remote sensors," *IEEE Access*, vol. 8, pp. 164775–164785, 2020.
- [8] S. Pala and D. G. Kurup, "A leading edge detection algorithm for ubw based indoor positioning systems," in *International Conference on Ubiquitous Communications and Network Computing*. Springer, 2021, pp. 45–55.
- [9] A. Ledergerber, M. Hamer, and R. D'Andrea, "Angle of arrival estimation based on channel impulse response measurements," in *2019 IEEE/RSJ International Conference on Intelligent Robots and Systems (IROS)*. IEEE, 2019, pp. 6686–6692.
- [10] I. Dotlic, A. Connell, H. Ma, J. Clancy, and M. McLaughlin, "Angle of arrival estimation using decawave dw1000 integrated circuits," in *2017 14th Workshop on Positioning, Navigation and Communications (WPNC)*, 2017, pp. 1–6.
- [11] T. Polonelli, S. Schlöpfer, and M. Magno, "Performance comparison between decawave dw1000 and dw3000 in low-power double side ranging applications," in *2022 IEEE Sensors Applications Symposium (SAS)*. IEEE, 2022, pp. 1–6.
- [12] L. Barbieri, M. Brambilla, A. Trabattoni, S. Mervic, and M. Nicoli, "Uwb localization in a smart factory: Augmentation methods and experimental assessment," *IEEE Transactions on Instrumentation and Measurement*, vol. 70, pp. 1–18, 2021.
- [13] H. Obeidat, W. Shuaieb, O. Obeidat, and R. Abd-Alhameed, "A review of indoor localization techniques and wireless technologies," *Wireless Personal Communications*, pp. 1–39, 2021.
- [14] Y. You and C. Wu, "Hybrid indoor positioning system for pedestrians with swinging arms based on smartphone imu and rssi of ble," *IEEE Transactions on Instrumentation and Measurement*, vol. 70, pp. 1–15, 2021.
- [15] K. Liu, Z. Tian, Z. Li, and M. Zhou, "Rfloc: A reflector-assisted indoor localization system using a single-antenna ap," *IEEE Transactions on Instrumentation and Measurement*, vol. 70, pp. 1–16, 2021.
- [16] P. Mayer, M. Magno, C. Schnetzler, and L. Benini, "Embeduwb: Low power embedded high-precision and low latency uwb localization," in *2019 IEEE 5th World Forum on Internet of Things (WF-IoT)*. IEEE, 2019, pp. 519–523.
- [17] Qorvo, "Dw3220," 2023, [Online; accessed 25-April-2023]. [Online]. Available: <https://www.qorvo.com/products/p/DW3220>
- [18] R. Juran, P. Mlynec, M. Stusek, P. Masek, M. Mikulasek, and A. Ometov, "Hands-on experience with uwb: Angle of arrival accuracy evaluation in channel 9," in *2022 14th International Congress on Ultra Modern Telecommunications and Control Systems and Workshops (ICUMT)*, 2022, pp. 45–49.
- [19] M. Stocker, H. Brunner, M. Schuh, C. A. Boano, and K. Römer, "On the performance of ieee 802.15.4z-compliant ultra-wideband devices," in *2022 Workshop on Benchmarking Cyber-Physical Systems and Internet of Things (CPS-IoTBench)*, 2022, pp. 28–33.
- [20] H. Friis, C. Feldman, and W. Sharpless, "The determination of the direction of arrival of short radio waves," *Proceedings of the Institute of Radio Engineers*, vol. 22, no. 1, pp. 47–78, 1934.
- [21] Z. Li, Z. Tian, and M. Zhou, "Decimeter level indoor localization using hybrid measurements of a distributed single receiver," *IEEE Transactions on Instrumentation and Measurement*, vol. 70, pp. 1–14, 2021.
- [22] D. Neunteufel, S. Grebien, and H. Arthaber, "Indoor positioning of low-cost narrowband iot nodes: Evaluation of a tdoa approach in a retail environment," *Sensors*, vol. 22, no. 7, 2022. [Online]. Available: <https://www.mdpi.com/1424-8220/22/7/2663>
- [23] L. Botler, M. Spörk, K. Diwold, and K. Römer, "Direction finding with uwb and ble: A comparative study," in *2020 IEEE 17th International Conference on Mobile Ad Hoc and Sensor Systems (MASS)*, 2020, pp. 44–52.
- [24] S. Bottigliero, D. Milanesio, M. Saccani, and R. Maggiore, "A low-cost indoor real-time locating system based on tdoa estimation of uwb pulse sequences," *IEEE Transactions on Instrumentation and Measurement*, vol. 70, pp. 1–11, 2021.
- [25] M. Heydariaan, H. Dabirian, and O. Gnawali, "Anguloc: Concurrent angle of arrival estimation for indoor localization with uwb radios," in *2020 16th International Conference on Distributed Computing in Sensor Systems (DCOSS)*, 2020, pp. 112–119.
- [26] A. F. Molisch, "Ultra-wide-band propagation channels," *Proceedings of the IEEE*, vol. 97, no. 2, pp. 353–371, 2009.
- [27] M. Stahlke, S. Kram, C. Mutschler, and T. Mahr, "Nlos detection using uwb channel impulse responses and convolutional neural networks," in *2020 International Conference on Localization and GNSS (ICL-GNSS)*. IEEE, 2020, pp. 1–6.
- [28] M. Naseri, A. Shahid, G.-J. Gordebeke, S. Lemey, M. Boes, S. Van de Velde *et al.*, "Machine learning-based angle of arrival estimation for ultra-wide band radios," *IEEE Communications Letters*, 2022.
- [29] D. Coppens, E. De Poorter, A. Shahid, S. Lemey, B. Van Herbruggen, and C. Marshall, "An overview of uwb standards and organizations (ieee 802.15. 4, fira, apple): Interoperability aspects and future research directions," *IEEE Access*, 2022.
- [30] M. Ghavami, L. B. Michael, S. Haruyama, and R. Kohno, "A Novel UWB Pulse Shape Modulation System," *Wireless Personal Communications*, p. 16, 2002.
- [31] T. Chen and C. Guestrin, "XGBoost: A scalable tree boosting system," in *Proceedings of the 22nd ACM SIGKDD International Conference on Knowledge Discovery and Data Mining*, ser. KDD '16. New York, NY, USA: ACM, 2016, pp. 785–794. [Online]. Available: <http://doi.acm.org/10.1145/2939672.2939785>



Tobias Margiani received his B.Sc and M.Sc degree in electrical engineering information technology from ETH Zürich, Zürich, Switzerland in 2021 and 2023, respectively. During his masters studies he spent one semester on exchange at the University of Texas at Austin, Austin TX, USA. His studies focused on embedded systems and communication technology, including indoor localization, UWB, IoT and fault tolerant systems.



Silvano Cortesi (S'22) received the B. Sc. and the M.Sc. degree in electronics engineering and information technology from ETH Zürich, Zürich, Switzerland in 2020 and 2021, respectively. He is currently pursuing the Ph.D. degree with the Center for Project-Based Learning at ETH Zürich, Zürich, Switzerland. His research work focuses on indoor localization, ultra-low power and self-sustainable IoT, wireless sensor networks and energy harvesting.



Milena Keller received the B.Sc and M.Sc degree in electrical engineering from ETH Zürich, Zürich, Switzerland in 2021 and 2023, respectively. She has experience in hardware design for high-frequency radio communication and a good expertise with the most recent indoor localization systems, such as UWB and trilateration. Moreover, she is gaining experience in wireless power transfer and magnetic levitation.



Christian Vogt (M'20) received the M.Sc. degree and the Ph.D. in electrical engineering and information technology from ETH Zürich, Zürich, Switzerland, in 2013 and 2017, respectively. He is currently a post-doctoral researcher and lecturer at ETH Zürich, Zürich, Switzerland. His research work focuses on signal processing for low power applications, including field programmable gate arrays (FPGAs), IoT, wearables and autonomous unmanned vehicles.



Tommaso Polonelli (M'20) received the M.Sc. degree and the Ph.D. in electronics engineering from the University of Bologna, Bologna, Italy, in 2017 and 2020, respectively. He is currently a post-doctoral researcher at ETH Zürich, Zürich, Switzerland. His research work focuses on wireless sensor networks, IoT, autonomous unmanned vehicles, power management techniques, structural health monitoring, and the design of ultra-low power battery-supplied devices with onboard intelligence.

He has collaborated with several universities and research centers, such as the University College Cork, Cork, Ireland, and the Imperial College London, London, U.K. He has authored over 40 papers in international journals and conferences.



Michele Magno (SM'13) is currently a Senior Scientist at ETH Zürich, Switzerland, at the Department of Information Technology and Electrical Engineering (D-ITET). Since 2020, he is leading the D-ITET center for project-based learning at ETH. He received his master's and Ph.D. degrees in electronic engineering from the University of Bologna, Italy, in 2004 and 2010, respectively. He is working in ETH since 2013 and has become a visiting lecturer or professor at several universities, namely the University of Nice Sophia, France, Enssat Lannion, France,

University of Bologna and Mid University Sweden, where currently is a full visiting professor at the electrical engineering department. His current research interests include smart sensing, low-power machine learning, wireless sensor networks, wearable devices, energy harvesting, low-power management techniques, and extension of the lifetime of batteries-operating devices. He has authored more than 220 papers in international journals and conferences. He is a senior IEEE member and an ACM member. Some of his publications were awarded as best papers awards at IEEE conferences. He also received awards for industrial projects or patents.